Prediction of long term strength of adhesively bonded steel/epoxy joints in sea water

M. Bordes[a, b], P. Davies[b, *], J.-Y. Cognard[c], L. Sohier[d], V. Sauvant-Moynot[a] and J. Galy[e]

[a] IFP, Lyon, Materials Department, 69390 Vernaison, France
[b] Materials & Structures Group, IFREMER Brest Centre, 29280 Plouzané, France
[c] LBMS, ENSIETA, 29806 Brest, France
[d] LBMS, Université de Bretagne Occidentale, 29285 Brest, France
[e] LMM-IMP, INSA Lyon, 69621 Villeurbanne, France

*: Corresponding author : P. Davies, Tel.: +33 298 22 4777; fax: +33 298 22 4535, email address : Peter.Davies@ifremer.fr

Abstract:

This study is concerned with the development of a tool to predict the long term behaviour of adhesively bonded steel joints aged in sea water. First, diffusion kinetics and the mechanisms governing the degradation of mechanical properties of an epoxy adhesive are described. These two sets of data were used in a coupled finite element (FE) analysis to determine the stress state in double lap shear (DLS) specimens before and after aging. However, subsequent tests on DLS specimens indicated an adhesive and not cohesive failure mode, so this approach could not be used to predict failure in the present case without introducing an interfacial damage parameter. A second approach was therefore employed, in which modified Arcan samples were designed in order to identify directly how the failure envelope changed with aging. Tests were performed on these modified Arcan specimens under shear, tensile/shear and tensile loads before and after aging. The results from these tests have enabled a tension–shear failure envelope to be constructed, which may be used to predict failure in joints with more complex stress states. The application of a coupled diffusion–mechanical property approach is illustrated for the Arcan specimen loaded in tension, and its application to the prediction of failure behaviour after aging is discussed.

Keywords: Durability; Aging; Finite element stress analysis; Coupling

1. Introduction

Adhesive bonding offers many advantages over traditional mechanical assembly and welding, and is used in many applications where weight is critical, such as land and air transport [1]. Adhesives are also used in many marine structures, for deck/hull assembly in pleasure boats for example, but additional precautions such as overlamination are usually taken to protect the joint. New applications are currently being envisaged on offshore platforms, particularly in areas where welding is not allowed for safety reasons, but in order to propose reliable solutions it is essential to be able to guarantee long term properties. Concern over the long term durability of joints in severe environments has been recognized as one of the factors which has limited more widespread application of adhesives [2], and in particular adhesives for marine [3] and offshore structures [4]. Several studies have focussed on wet aging of adhesive joints. Humid environments can be very severe, resulting in reversible or permanent changes to the adhesive (plasticization, swelling, hydrolysis) [5-7], and to the substrate/adhesive interface (corrosion, cracking, debonding, etc.) as described by Bowditch and others [8,9]. As a result, much work has been devoted to characterizing the durability of bonded joints. In the aeronautical industry durability testing has relied on the Boeing wedge test [10]. Popineau and Shanahan [11] used this specimen geometry to study an aluminium-composite assembly and to link the assembly fracture energy to the adhesive water uptake. Fernando and Harjopayitno [12] used TDCB (Tapered Double Cantilever Beam) specimens to measure the assembly fracture energy using fatigue tests and aging in distilled water.

There have been few studies specifically directed at the marine industry. Knox and Cowling [13] tested thick adherend shear test specimens in a salt water environment during 8 years and measured the influence of spew fillet on joint durability. Gontcharova et al. studied steel/composite joints [14,15] and evaluated aging under laboratory conditions and at sea, studying how loading affects aging performance.

Crocombe and colleagues have worked extensively on durability modelling [16-18] and point out that in order to be able to predict how aging will affect the long term behaviour of adhesively bonded structures it is first necessary to have two sets of data:

diffusion data for the adhesive, and

moisture-dependent mechanical properties of the adhesive.

If these data can be correctly integrated into a coupled structural analysis it should be possible to predict how a bonded joint will perform, provided the failure mode remains mainly cohesive (i.e. within the adhesive). If the mode of failure changes with aging then additional data on interface characteristics will be required. These may include swelling data for the adhesive and/or interface degradation parameters, but in the first approach considered here these are neglected. Finally, in order to validate such a model a third set of data, describing the influence of aging on the joint properties is then required. Figure 1 shows a schematic representation of the methodology.

2. Materials

The adhesive studied is a two-part epoxy system, Araldite 2015 from Huntsman Advanced Materials (Everberg, Belgium). This is a DGEBA based epoxy with an amine hardener. The cure cycle recommended by Huntsman and applied here is 24 hours at room temperature followed by a post-cure at 80°C for 1 hour. The glass transition temperature (Tg) value of the bulk adhesive was measured by DSC (differential scanning calorimetry) and the average value was 75 ±4°C. The Tg of the adhesive in a bonded assembly was also measured, and a value of 74°C was obtained, suggesting that the cure state of the adhesive was similar for both. The substrate is a low carbon steel (S235 according to French standard NF 10025), a grade widely used offshore. For modeling the steel properties used were an elastic modulus of 212 GPa and a Poisson's ratio of 0.28. The surface treatment was grit blasting with

corundum (*Rugos 2000,* 20/30 grade, spherical particles ϕ=0.3-1.8 mm). The roughness obtained was characterized as R_a=12 $\pm$ 2.6 μm (R_z = 67.1 $\pm$ 12.8 μm) (characterized using the ISO 3274 standard with a cut-off value of 1.5 mm).

3. Aging conditions and mechanical tests

Aging on bulk adhesive was performed in de-ionised water salt and sea water at three temperatures, 20, 40 and 60°C. Water uptake was measured by gravimetry on samples with dimensions of 1.5x15x80 mm^3. Tensile tests were performed at 1 mm/minute on "dog-bone" specimens (type 1BA in ISO standard 527-2) aged under the same conditions to measure the influence of water uptake on adhesive mechanical properties.

Two environments were used to age adhesively bonded DLS and Arcan specimens, de-ionised water (aging temperatures: 20 and 60°C) and natural seawater in the laboratory (aging temperature: 20°C). Tests on bonded joint specimens were performed under displacement control at a rate of 1mm/minute. Image analysis of the specimen edges was used to measure local displacements for both DLS and Arcan tests, as described previously [19]. Fine paint spots were sprayed onto the surface and image correlation was used to measure the displacements of the substrates.

4. Bonded joint specimen geometries

Table 1 presents the bonded joint specimen geometries tested here and their dimensions. The DLS geometry is widely used and a standard geometry has been defined (ASTM D3528), but tensile loading results in a complex stress state. The specimens used here were therefore analysed numerically, in order to quantify this stress state for the substrates and adhesive tested. The Arcan specimen has been used elsewhere [19-21] but the geometry used here was specifically designed for this study, and will be discussed below.

5. Weight gain studies to determine the diffusion model

A series of weight measurements on bulk adhesive specimens resulted in the plots shown in Figure 2. These indicate the weight change ((w_t, the weight at time t – initial weight, w_o)/w_o) as a percentage, plotted versus $t^{1/2}$ x S/V, where t is the time in days, S the sample surface area and V the sample volume.

The bulk adhesive absorbs more de-ionised water than salt water for the same aging time. The absorption of de-ionised water appears to reach a saturated level at 8.4% at 60°C and 7% at 20°C, while the adhesive re-absorbs salt water after a first stabilisation plateau near 4.5%. At 20°C, the absorption of salt water (water + 3.5 wt% NaCl) and seawater is equivalent. We attribute this behaviour to osmotic degradation occurring at the interfaces between polymer matrix and mineral fillers of the adhesive [22]. Osmotic degradation is a creation of cavities under the influence of an osmotic pressure. This osmotic pressure occurs between two solvents with different chemical activities, as in the specimen which contains small molecules and the aging water.

The diffusion of water was modelled by a Fickian law using Equation (1) [23] for the complete absorption of deionised water and the first part of absorption of salt water (Figure 2).

$$\frac{wt}{w\infty}=1-\left(\frac{8}{\pi^2}\right)^3\left[\sum_{m=0}^{\infty}\sum_{n=0}^{\infty}\sum_{p=0}^{\infty}\frac{\exp(-1.q_{mnp})}{(2m+1)^2\,(2n+1)^2(2p+1)^2}\right] \text{ with}$$

$$q_{mnp}=D.\frac{\pi^2}{4}\left[\left(\frac{2m+1}{e/2}\right)^2\left(\frac{2n+1}{L/2}\right)^2\left(\frac{2p+1}{l/2}\right)^2\right](1)$$

where w_t is the weight at time t, w the weight at saturation, D is the diffusion coefficient, e the thickness, l the length, and L the width.

6. Diffusion modelling

Using the Fickian model it is possible to calculate the water concentration at any point in the adhesive at any time for different samples. Figure 3a shows an example of concentration profiles for the DLS joint, modelled using *Comsol Multiphysics™* software from Comsol (Stockholm, Sweden). The water diffusion in the adhesive thickness of the assembly with dimensions 12.5 x 24 x 1 mm^3 was modelled in three dimensions with a cubic mesh. The behaviour was Fickian, with the average diffusion coefficient determined previously (see Table 2), and we considered that the concentration was equal to 1 on the surfaces around the edges and to zero at the upper and lower surfaces. A water concentration map within the adhesive can be obtained, and we can determine the evolution of weight gain of the adhesive in the assembly, by integrating the concentration over the adhesive volume. This analysis provides an indication of the time necessary to saturate the joint provided there is not accelerated water ingress along the steel/adhesive interface region. This is very useful for planning test schedules and here it is apparent that the time required to reach saturation is much faster at 60°C than at 20°C but very long in both cases, Figure 3b. For the aging times in this study (and indeed for most published studies), saturation of the adhesive is not attained. As a result it is necessary to consider the concentration and mechanical property gradient in the adhesive.

7. Influence of water on the mechanical properties of the adhesive

A series of tensile tests enabled the dependence of tensile properties on water content (for both sea water and de-ionised water) to be determined. The water content was determined by simulation of water diffusion in the central part of the dog-bone sample using *Comsol Multiphysics* software. Figure 4 shows the results for adhesive modulus and yield stress plotted versus the simulated amount of water. The average diffusion coefficients calculated previously (Table 2) were used. Here, the yield stress value was defined as the end of linearity of the tensile stress-strain plot. These two parameters decrease with water uptake, with no clear influence of the environment (de-ionised or salt water). They are represented as a function of a weight uptake normalized by an average saturation value of 8.4 wt% for the aging temperature of 60°C and 7% for the aging temperature of 20°C. The drop of these parameters is due to two mechanisms: the plasticization of the adhesive by water (a reversible effect), and the osmotic degradation at the polymer matrix-filler interfaces (observed in microscopic studies elsewhere). Based on these data, it is possible to determine how the stiffness and the yield stress vary throughout the joint during immersion.

8. Numerical stress analysis of DLS specimens

In order to examine the DLS specimens studied here in more detail a numerical analysis was performed, using *CAST3M* finite element software from CEA (Saclay, France). The FE

modelling is performed in 2D plane stress with a fine quadrilateral mesh (80 linear elements) in the adhesive thickness. The geometry of the specimen is shown in Figure 5. Figure 6 shows the evolution of the components of the stress and of the von Mises equivalent stress through the thickness of the adhesive. The graphs correspond to different positions in the adhesive; y = 0 represents the average line of the adhesive and y = ± e (e = $h_2/2$) are lines close to the adhesive-substrate interfaces (upper and lower). For a given line in the adhesive (given y), the stress component is represented on the y-axis along the overlap length (x ∈ [-$l_2/2$, $l_2/2$]). For these plots, the stress is normalized in order to obtain a shear stress equal to 1 at the centre; moreover at the centre the von Mises equivalent stress is also normalized to 1.

As has been shown previously by many authors [1,24,25] there are significant edge effects for this specimen. The point A (Figure 5) is the most highly loaded due to the load transfer path associated with the asymmetric geometry and the local geometry. The von Mises stress at the point A is 5 times higher than the joint center stress. The most significant stress is the yy component. Indeed, bending of the outer substrates accentuates the peel stress concentration at the ends of the overlap. It is the adhesive-central substrate interface (line A-B) which sees the highest stress value, and this is often the weakest point of the assembly. Fracture can occur easily at this point due to defects or surface treatment variability. Therefore, we will concentrate on this interface for the study of the aged assembly.

9. Results from tests on aged DLS joints

Table 3 shows the aging conditions applied to the DLS specimens. Tests were performed on DLS joints aged for periods up to one year. Figure 7 (a) and (b) shows the apparent failure stresses (failure load/measured bonded area) versus aging time and simulated weight gain respectively, and it is clear that they decrease significantly after aging. For aging in de-ionised water, the decrease is faster at 60°C than at 20°C, and the strength decrease is slower in seawater than in de-ionised water. Figure 7(b) confirms that the joint strength decrease of the DLS is due to the water uptake of the adhesive. Although there is some variability in the measurements, there appear to be two steps in the DLS strength decrease. There is a first step for which the stress decreases to an average of 8 MPa and stabilises between 1.2 % and 5.5% weight gain. Then there is a second decrease and stabilisation between 5.5% and 8.2% at 6 MPa. Knowledge of the overall weight gain alone is not sufficient to define the aging behaviour of the DLS specimen. In order to interpret this behaviour it is necessary to know the water concentration gradient in the adhesive (Figure 8(a)) and how the stress state changes with water ingress. Figure 8 (b) shows how water will affect local stiffness, but when the DLS specimen is loaded this must be considered with respect to the non-uniform stress state introduced. The von Mises stress at the interface AB of the assembly (Figure 5) is shown at different aging times for the two aging temperatures (Figure 8 (c) and (d)). Initially, the stress concentrations are very high at the end of the joint. These are reduced by water towards a more uniform stress state. This change in stress states for different aging times may be responsible for the two levels of strength noted previously (Figure 7 (b)).

In parallel with these changes in stress distribution, the strength of the adhesive also changes, decreasing as water arrives. The failure locus will depend on the relative changes of stress concentration and strength at each point in the adhesive. It would, therefore, not be unexpected that an initial improvement in joint performance be noted, as stress concentrations are reduced, followed by a gradual decrease in strength as the adhesive strength drops. In the unaged state, the fracture is located close to the interface but a fine layer of adhesive remains on the substrate (Figure 9a), so the fracture is cohesive but located very near the substrate-adhesive interface. It is interesting to note that the fracture is

located at the interface AB (Figure 5), which confirms the influence of the edge effects on fracture as indicated by the modelling. However, as aging proceeds (from 3 months of aging), the fracture surfaces become truly interfacial, with very little adhesive visible on the substrate surface (Figure 9b). In addition to the degradation of the adhesive properties, there is also degradation of the interface during aging of the DLS assembly.

As we can see, the stress state in the adhesive, at the interface with the substrate, has certainly an influence on the fracture at this interface, but additional information on the interface behaviour is needed. This means that the approach proposed initially by Crocombe [2] cannot be applied directly to predict failure here. This poses a number of difficulties as the complex stress state in the DLS specimen and its evolution during aging would require knowledge of interface properties over a range of loading conditions. While some stress-based tests are available to characterize interfaces [26,27], it may be easier to employ fracture mechanics tests so that traction responses can be identified for interface elements to address this problem [28,29].

In the present work, an alternative approach was adopted by employing a specimen geometry which allows joints to be loaded under simpler conditions. The modified Arcan specimen was adopted, in order to identify the influence of water on the failure envelope directly, for joints prepared under identical conditions (same substrates and preparation, same cure cycle). Arcan specimens have been used successfully in previous studies of epoxy bonded aluminium assemblies [19] but some modification was needed for this aging study.

10. Development of an Arcan specimen geometry

Previously, Arcan specimens have been designed with beaks (Figure 10), which ensure a more uniform stress state by significantly reducing stress concentrations at the edges [19,21]. These have been used extensively for characterization of aluminium assemblies. In the present study the substrates were steel and the grit blasting operation was imposed, as this is currently used for paint operations on offshore platforms. This is a very aggressive surface treatment and preliminary tests indicated that the machined beaks would not resist it, so a specimen with "inverse beaks" was developed, as shown in Figure 10. In order to optimise the specimen geometry numerical stress analysis was used (plane stress 2D) with *CAST3M* FE software. Figure 11 shows the results from these analyses for a 0.5 mm adhesive thickness (2e).

Compared to the DLS configuration, the Arcan inverse geometry significantly reduces edge effects (Figure 6), more details can be found in [30]. This geometry was therefore adopted for the aging tests. Figure 12 shows the test fixture and the substrate profile, with a rounded chamfer of 0.2 mm height and 0.5 mm length. The bonded assembly sample is clamped in the central section of the fixture, and by varying the angle γ from 0° to 90° the loading can be changed from tensile to shear (Figure 12). The main advantage of using the modified Arcan fixture rather than the DLS is that the initial unaged stress state is much more uniform, so data from unaged samples can be used for design. As will be shown below, the effect of water ingress is still complex, but simpler than for the DLS specimen.

Figure 13 shows stress-deformation plots for the two assemblies DLS and Arcan (shear loading) in the unaged state. DT and DN (used in Figure 13 and 14) are respectively the tangential and normal relative displacements of the two interfaces substrate/adhesive. The normal direction is defined as the normal to the mean plane of the adhesive. FT and FN are the normal and tangential components of the applied force. The DLS has a very similar initial response to the Arcan specimen. However, at stresses above 10 MPa the slope changes for the DLS and the assembly failure occurs at 15 MPa. For the Arcan assembly failure occurs at a much higher stress, around 30 MPa. This underlines the strong influence of the stress concentration at the DLS edges.

11. Results from aging of bonded Arcan joints

Table 4 shows the different aging conditions applied to the Arcan specimens. Figure 14 shows the influence of aging on the response of Arcan samples tested at 0° (tension), 45° (tension/shear) and 90° (shear). It is clear that water affects the behaviour of the assembly under all three loading conditions. For all loading directions, the strength of the assembly drops by approximately 50% after both aging durations. There is little difference between 1 month and 3 months aging. However, the force-deformation plots are dependent on the loading conditions. Under tensile loads, the stiffness of the assembly changes very little with aging, only the yield and fracture loads drop. In pure shear and tension-shear, the adhesive water uptake decreases the stiffness and the yield stress of the assembly and the adhesive strain to failure increases. This kind of behaviour was also seen in the tensile tests performed on the aged bulk adhesive. It may be noted that DT for shear loading is nearly ten times DN for tensile loading.

From the plots in Figure 14 it is possible to extract the stress corresponding to onset of plasticity, (averaged over the specimen surface) and the failure envelopes. Figure 15 shows examples of the average stress values corresponding to the end of linearity (yield stress) and final failure before and after aging for the three loading types. More load combinations would be needed to give a more accurate envelope. These provide a global indication of how aging in water affects the joint response under the three loading conditions, but to use these curves directly is to assume that the stress state induced in the specimen remains homogeneous. In this case, there are not large stress concentrations at the specimen edges initially, so the effect of the water is simply to reduce the edge stresses further as stiffness drops. While not simple, this is a less complex case to analyse than the DLS. The example of tensile loading is considered in detail below, as for this loading case failure was cohesive in the unaged state, as shown in Figure 16. After aging for one month, an adhesive fracture in the thicker (chamfered) edge region of the adhesive is visible. Fracture initiation in this area may explain why similar performance was measured for both aging times. The shear specimens also show some adhesive fracture after aging.

The Arcan specimen was modelled under tensile loading with the *Comsol Multiphysics* software, in a coupled model taking water diffusion into account. A complete simulation of this problem requires 3D models with refined meshes in order to obtain reliable results for the stress distribution in the adhesive, but such simulations are too complex for a first analysis. Thus, only a section in the width of the specimen was modelled in 2D, to obtain a first estimation with an elastic behaviour assumption. As the analyses of the Arcan results only take the normal stress into account, here it seems appropriate to use a plane stress condition for modelling, as plane strain conditions often overestimate the stress compared to 3D calculations. The plane strain conditions block displacements in the third direction (which is not exactly representative of the real problem) and result in an elevated stress in this direction. Several recent papers have examined model assumptions [31,32], the aim here is primarily to reveal changes with aging, not to present quantitative stress predictions. Numerical results presented below were therefore obtained under plane stress conditions with refined meshes (30 elements along the adhesive half-thickness).

The aim is to determine the applied force or stress at which the first plastic strain will occur in this assembly. It is therefore necessary to compare the maximum stress value calculated at all points to the yield stress of the adhesive. The von Mises stress was used, though it is recognized that other equivalent stress values could be used, and that the influence of hydrostatic pressure on yielding should be included in a more refined approach [33,34]. Figure 17a shows the water concentration profiles and Figure 17b the resulting adhesive modulus evolution in the adhesive (based on the data in Figure 4a) for the different aging conditions. The modulus decreases rapidly to a low value. Figure 18 (a) shows the von Mises stress at the adhesive/substrate interface for a unit applied load. At the first diffusion times considered (1 day and 1 month), the stress at the edges decreases while it increases at the

centre. Then, as the modulus becomes more uniform, the tendency is reversed, but the highest stress is always at the centre.

The appropriate yield stress is obtained by calculating the water content at all points and using the relation between yield stress and water content in Figure 4b. Figure 18b shows the ratio (α) of yield stress divided by the von Mises stress along the joint for different aging times. We can see that the first yielding will occur at the centre of the joint, as the lowest ratio is found there throughout aging, apart from a small local effect at the chamfer after one day. The ratio α (or safety factor) decreases with water uptake. Figure 19 shows that the evolution of this ratio with aging time is similar to the evolution of the experimental tensile yield stress (Figure 15a) over the same period.

This provides a first indication of what happens in the tensile loaded Arcan assembly, but the adhesive fracture in the chamfer zone (Figure 16) suggests that there may also be some degradation of interfacial bonding. Further work is now needed to enrich the coupled model, to integrate the changes in the interfacial region observed with aging, as shown in Figure 1. Various factors may influence this interfacial response, including adhesive swelling and corrosion. The viscoelastic behaviour of the adhesive may also need to be included in the analysis. A complete analysis of the influence of aging on the non linear behaviour of the adhesive, starting from the experimental results obtained with the modified Arcan fixture, requires the development of 3D non-linear models with refined meshes. Moreover, the development of a model representing the influence of water diffusion on the non-linear mechanical behaviour requires inverse identification using time dependent non-linear FE simulations. Thus, it could be interesting to analyse bonded specimens with protections on the long sides to validate 2D models, in order to limit the complexity and the numerical cost. The number of factors which influence the durability of bonded assemblies is so large that simplifying assumptions are essential. The results shown here suggest that in some cases (such as tensile loading of the Arcan sample) the adhesive behaviour can be used to provide a useful first indication of the evolution of the long term strength.

Conclusion

This paper presents results from aging tests on both traditional double lap shear specimens and a new modified Arcan specimen. Both show a significant drop in strength after immersion in water. A coupled analysis, based on a diffusion model and an experimentally determined relationship between water content and adhesive property loss, has been used to analyse the stress state in the specimens during aging. This clearly shows the difficulties in interpreting DLS data as the position of maximum stress concentration varies with aging. The modified Arcan specimen is preferable, it provides a much more uniform initial stress state, and a detailed study of the tensile loading case has shown how coupled analysis can be used to examine the long term response of aged structures in water. However, further model development is needed to include the complex mechanisms observed on aged specimens.

References

Adams, R.D., Comyn, J. and Wake, W.C, Structural adhesives joints in engineering, Chapman & Hall, 2nd edition, 1997.
Crocombe AD, 'Durability modelling concepts and tools for the cohesive environmental degradation of bonded structures', Int J. Adhesion and Adhesives, 17, 1997, 229-238.
Jarry E, Shenoi RA, 'Performance of butt strap joints for marine applications', Int. J. Adhesion & Adhesives, 26, 2006, 162-176.
Cowling MJ, HSE report P3384, A review of adhesive bonding for offshore structures, 1997

Ellis T.S. and Karasz F.E.**,** 'Interaction of epoxy resins with water: the depression of glass transition temperature' Polymer, 1983, 25, 64

Popineau, S., Rondeau-Mouro, C., Sulpice-Gaillet, C., Shanahan, M. E. R., 'Free/bound water absorption in an epoxy adhesive' Polymer, 2005, 46, 10733

Xiao, G. Z. and Shanahan, M. E. R., **'**Water absorption and desorption in an epoxy resin with degradation' J. Poly. Sci. B, 1997, 35, 2659

Bowditch MR, 'The durability of adhesive joints in the presence of water, Int J. Adhesion and Adhesives', 1996, 16, 73-79.

Kinloch AJ, Durability of Structural Adhesives, Applied Science Publishers, 1983

Hart-Smith LJ, 'Adhesive bonding of composite structures – Progress to date and some remaining challenges', J. Comp Tech & Research 24, 2002, 3, 133-153.

Popineau, S. and Shanahan, M.E.R., **'**Simple model to estimate adhesion of structural bonding during humid ageing' Int. J. of Adhesion and Adhesives, 2006, 26, 363

Fernando M., Harjoprayitno W.W., 'A fracture study of the influence of moisture on the fatigue behaviour of adhesively bonded aluminium-alloy joints', Int. J. of Adhesion and Adhesives, 1996, 16, 113-119

Knox, E. M. and Cowling, M. J., 'Durability aspects of adhesively bonded thick adherend lap shear joints', Int. J. of Adhesion and Adhesives, 2000, 20, 323

Roy, A., Gontcharova E., 'Hygrothermal effects on failure mechanisms in composite/steel bonded joints', ASTM STP 1357, 2000, 353-371

Davies P, Roy A, Gontcharova E, Gacougnolle JL, Accelerated marine aging of composites and composite/metal joints, Proc DURACOSYS 99, ed Cardon et al., Balkema, 2000, 253-258.

Loh W.K., Crocombe A.D., Abdel Wahab MM, Ashcroft IA, 'Environmental degradation of the interfacial fracture energy in an adhesively bonded joint', Eng Fracture Mechanics, , 2002, 69, 2113-2128

Abdel Wahab M.M., Crocombe A.D., 'Coupled stress-diffusion analysis for durability study in adhesively bonded joints', Int. J. of Adhesion and Adhesives, 2001, 22, 61-73

Hua Y., Crocombe A.B., 'Continuum damage modelling of environmental degradation in joints bonded with EA9321 epoxy adhesive', Int J of Adhesion and Adhesives, 2008, 28, 302-313.

Cognard JY, Davies P, Sohier L, Créac'hcadec R. 'A study of the non-linear behavior of adhesively-bonded composite assemblies', Composite Structures 2006; 76: 34-46.

Arcan, L., Arcan, M. and Daniel, I., 'SEM fractography of pure and mixed mode interlaminar fracture in graphite/epoxy composites', ASTM Tech. Publ., 1987, 948, 41-67.

Cognard, J.Y., Davies, P., Gineste, B. and Sohier, L., 'Development of an improved adhesive test method for composite assembly design', Composite Science and Technology, 2005, 65, 359-368.

Coeuille, F., 'Polymer coatings of fluid pipes : characterization and evolution of the adhesion in aggressive environment', PhD Thesis, Ecole des Mines de Paris, 2002.

Crank J, The Mathematics of Diffusion, Oxford University Press 1975 , 2nd edition

Tsai MY, Oplinger DW, Morton J, 'Improved theoretical solutions for adhesive lap joints', Int J Solid Stuct., 1998, 35, 12, 1163-1185.

Xiao XS, Foss PH, Schroeder JA, 'Stiffness prediction of the double lap shear joint. Part 2: Finite element modeling', Int J. Adhesion and Adhesives, 24, 3, 2004, 239-246

Roche AA, Bouchet J, Hamelin P, 'Internal stresses, Young's modulus and practical adhesion of organic coatings applied onto 5754 aluminium alloy', Thin Solid Films, 1999, Vol. 355-356, 270-276.

Bouchet J, Roche AA, 'The formation of epoxy/metal interphases: mechanisms and their role on practical adhesion'. Journal of Adhesion, 2002, 78, 799-830

Crocombe A.D., Hua Y.X., 'Predicting the residual strength for environmentally degraded adhesive lap joints', Int. J. of Adhesion and Adhesives, 2006, 26, 325-336.

Liljedahl CDM, Crocombe AD, Wahab MA, Ashcroft IA, 'Modelling the environmental degradation of adhesively bonded aluminium and composite joints using a CZM approach', Int. J. of Adhesion and Adhesives, 27, 2007, 505-518.

[30] Cognard J.Y., "Numerical analysis of edge effects in adhesively-bonded assemblies - Application to the determination of the adhesive behaviour", Computers & Structures, Vol 86, pp 1704-1717, 2008

[31] Goncalves JPM, de Moura MFSF, de Castro PMST, A three dimensional finite element model for stress analysis of adhesive joints, Int J. Adhesion and Adhesives, 2002, 22, 357-365.

[32] Da Silva LFM, des Neves PJC, Adams RD, Spelt JK, Analytical models of adhesively bonded joints – Part 1 : Literature survey, Int J. Adhesion and Adhesives, 29, 2009, 319-330.

[33] Wang CH, Chalkley P, Plastic yielding of a film adhesive under multiaxial stress, Int J. Adhesion and Adhesives, 20, 2000, 155-164.

[34] Dean G, Crocker L, Read B, Wright L, Prediction of deformation and failure of rubber-toughened adhesive joints, Int J. Adhesion and Adhesives, 24, 2004, 295-306.

Tables

Table 1. Joint specimen geometries

Type	Substrate thickness (mm)	Overlap/Width (mm)	Adhesive Thickness (mm)	Loading
Double Lap Shear	5	12.5 / 24	1 ± 0.1 mm	- Tension
Arcan	20	66 /10.5	0.6 ± 0.1 mm	-Tension -Tension/shear -Shear

Table 2. Diffusion coefficients used in modelling.

Temperature	D (m².s^{-1})	
	De-ionised water	Salt water
20°C	$4.69 \pm 1.85 \ 10^{-14}$	$8.02 \pm 3.17 \ 10^{-14}$
40°C	$2.20 \pm 0.87 \ 10^{-13}$	-
60°C	$1.15 \pm 0.45 \ 10^{-12}$	$1.38 \pm 0.54 \ 10^{-12}$

Table 3. DLS joint aging conditions.

Specimen	Aging	Duration (months)	Number of specimens	Test load
DLS	De-ionised 20, 60°C Seawater 20°C	0, 1, 3, 6, 12 0, 0.5, 1, 3, 6	5 for unaged state, 2 per aging condition	Tensile

Table 4. Bonded Arcan joint aging conditions

Specimen	Aging	Duration (months)	Number of specimens	Load angle γ (see Fig. 12)
Arcan	Seawater 60°C	0, 1, 3	4 per condition for each loading type (total 36)	0, 45, 90°

Figures
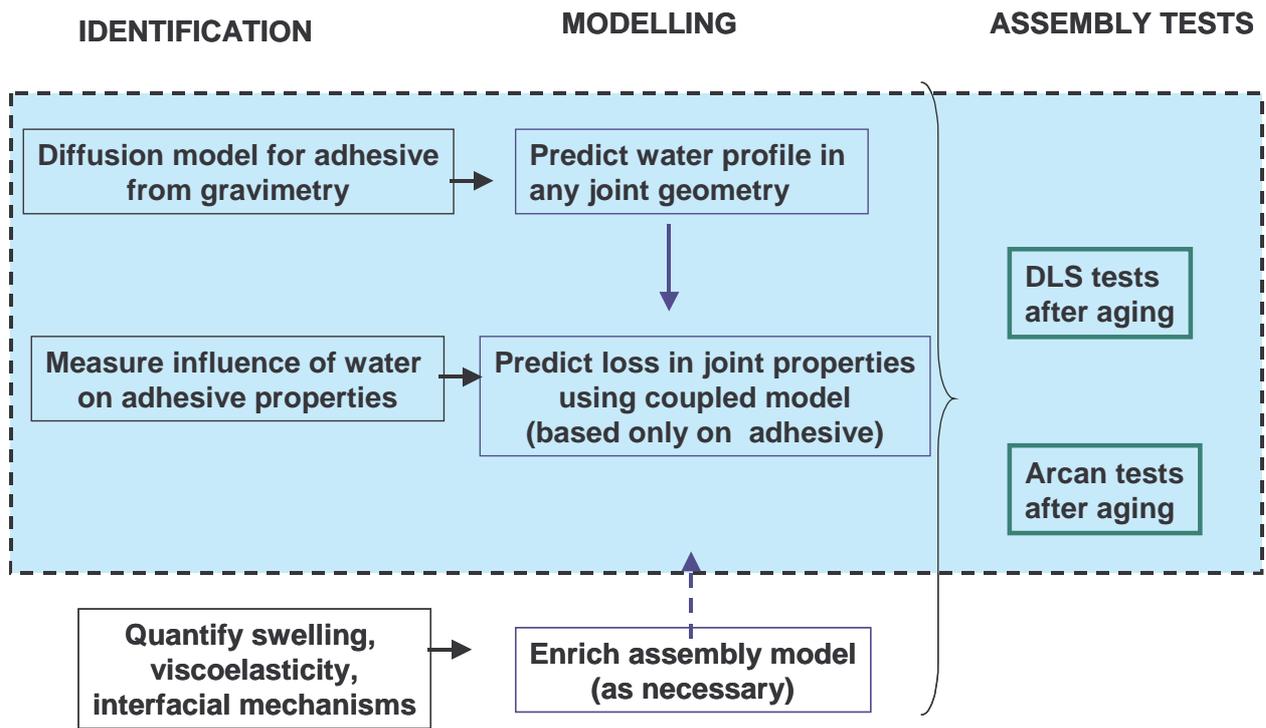
Figure 1. Schematic representation of methodology to predict assembly strength after aging. The dashed line indicates the points addressed in this paper.

(a)

(b)
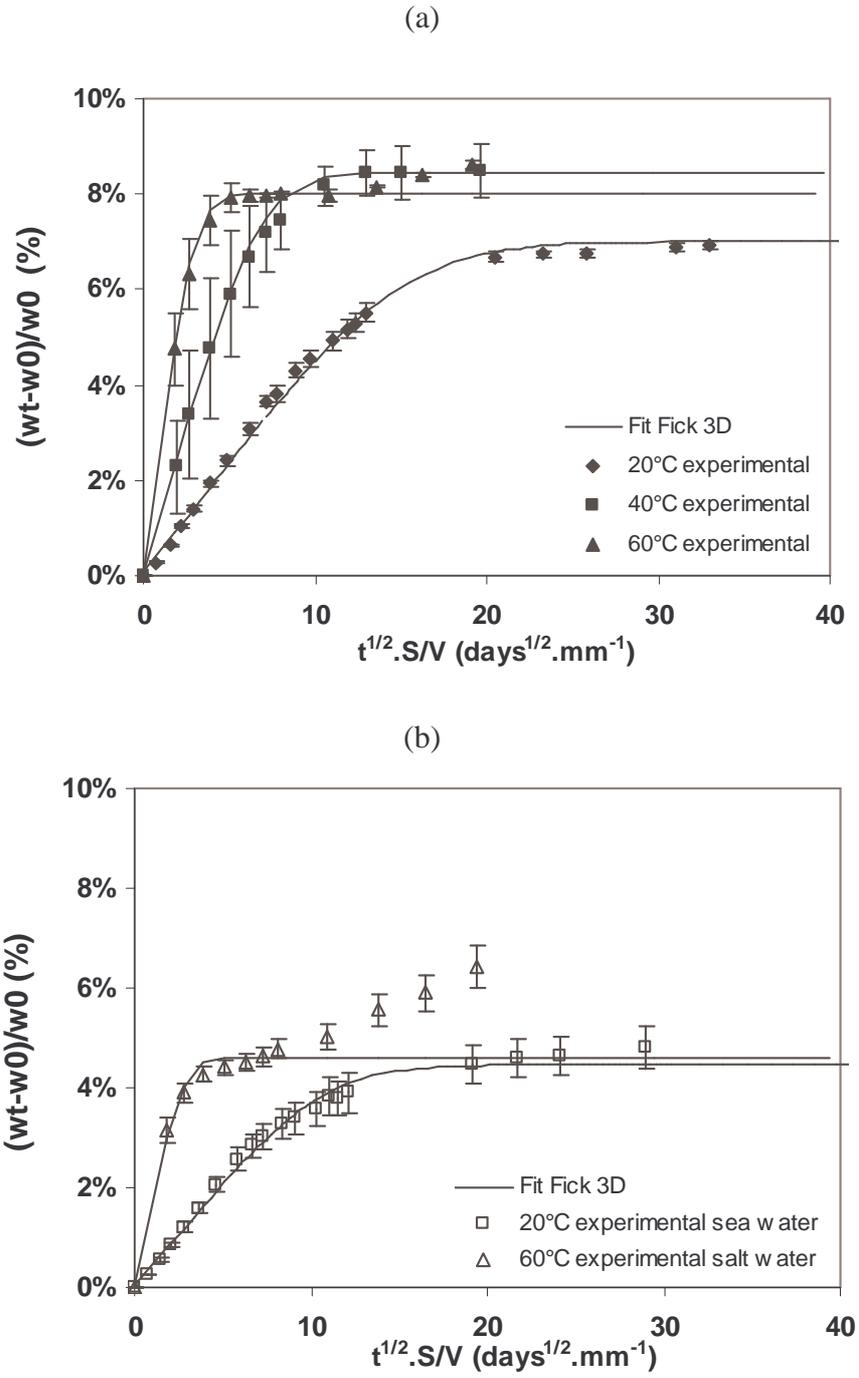
Figure 2. Water uptake of Araldite 2015 in (a) deionised water at 20, 40 and 60°C, and (b) seawater, at 20 and 60°C, with Fickian model plots.

(a)

(b)
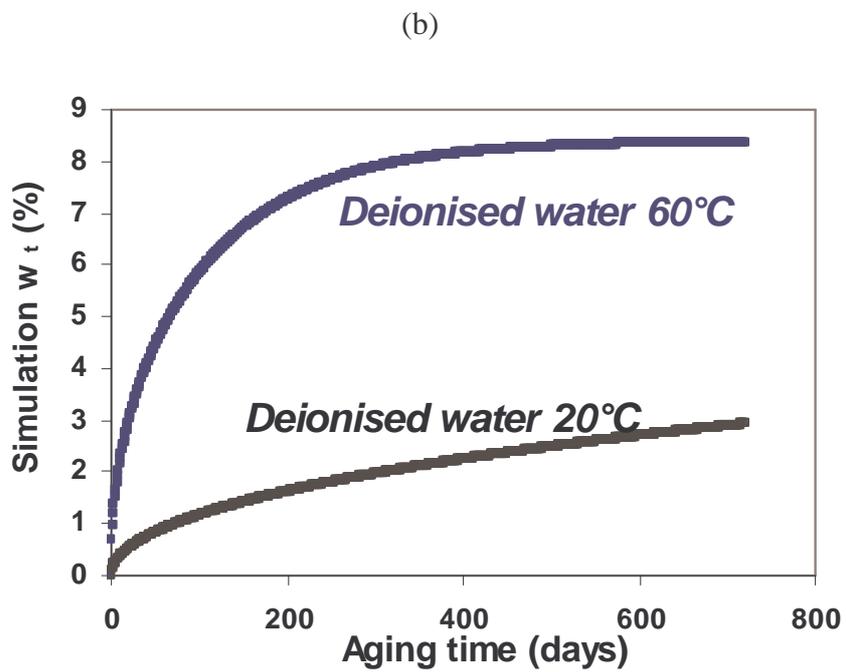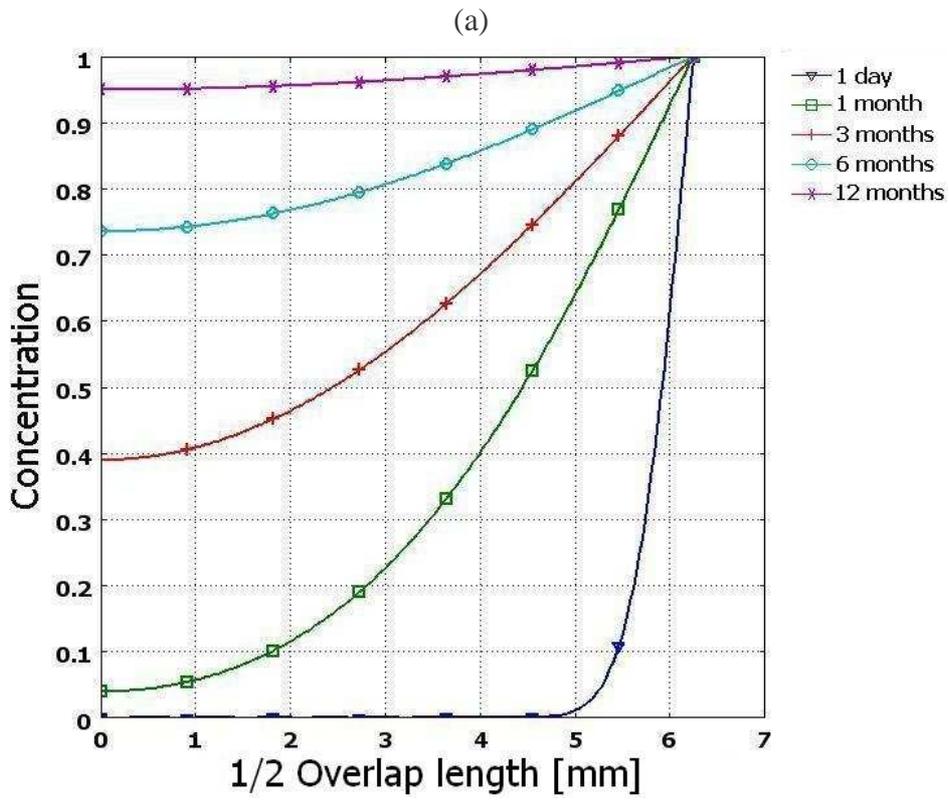
Figure 3. Simulation of diffusion into the adhesive of a DLS assembly.
(a) sea water profile at 60 °C, (b) comparison between simulations for deionised water at
20°C and 60°C.

(a)

(b)
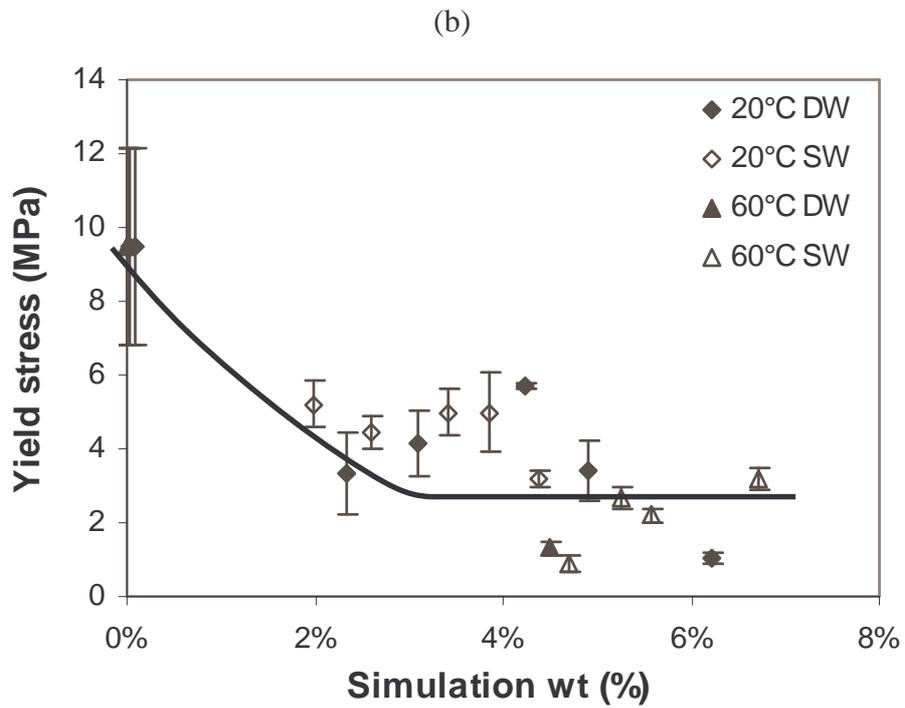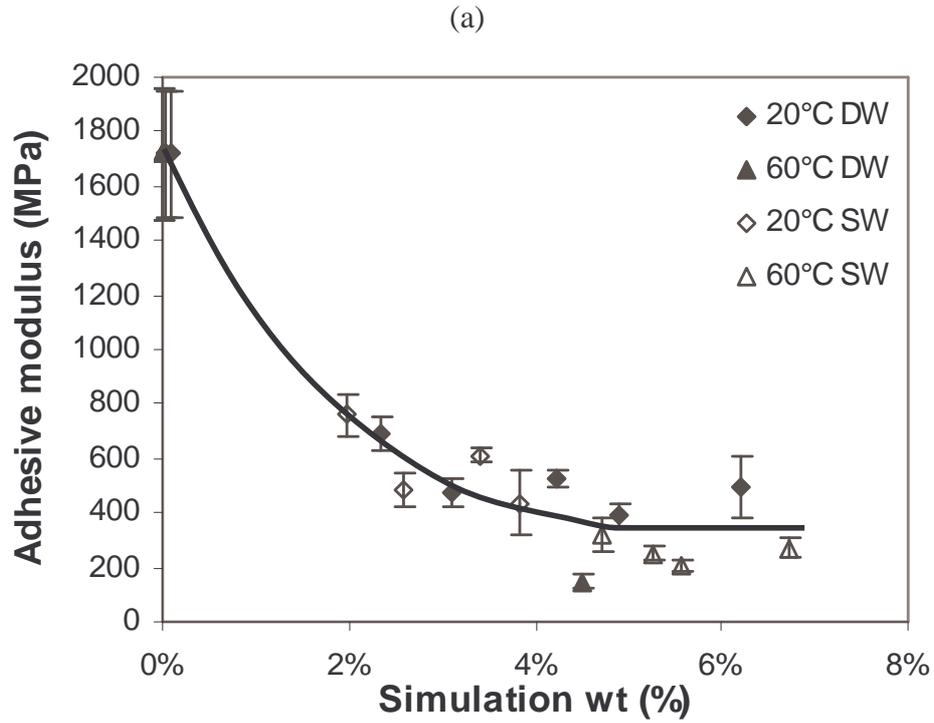
Figure 4. Modulus (a) and yield stress (b) evolution versus the % weight obtained by
numerical simulation, DW (de-ionised water) and SW (salt water)
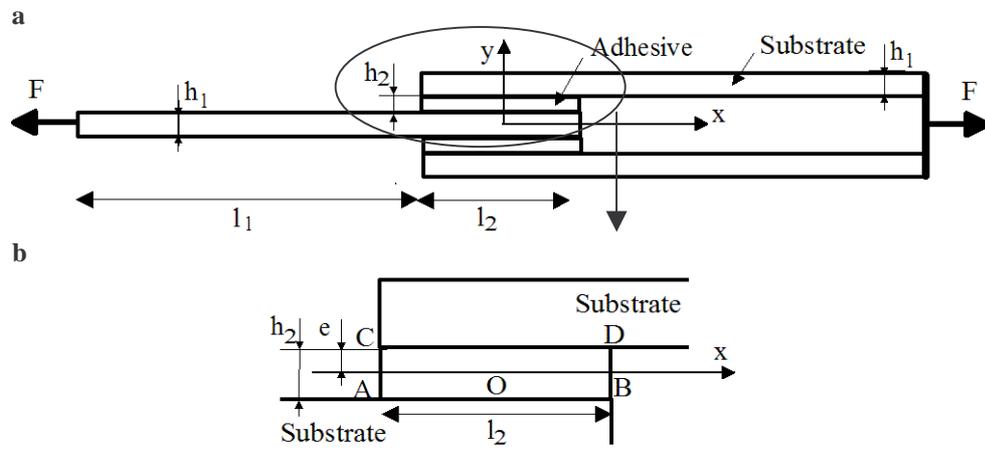
Figure 5. Geometry of the double lap shear specimen. (a) geometry, (b) zoom of the central section.
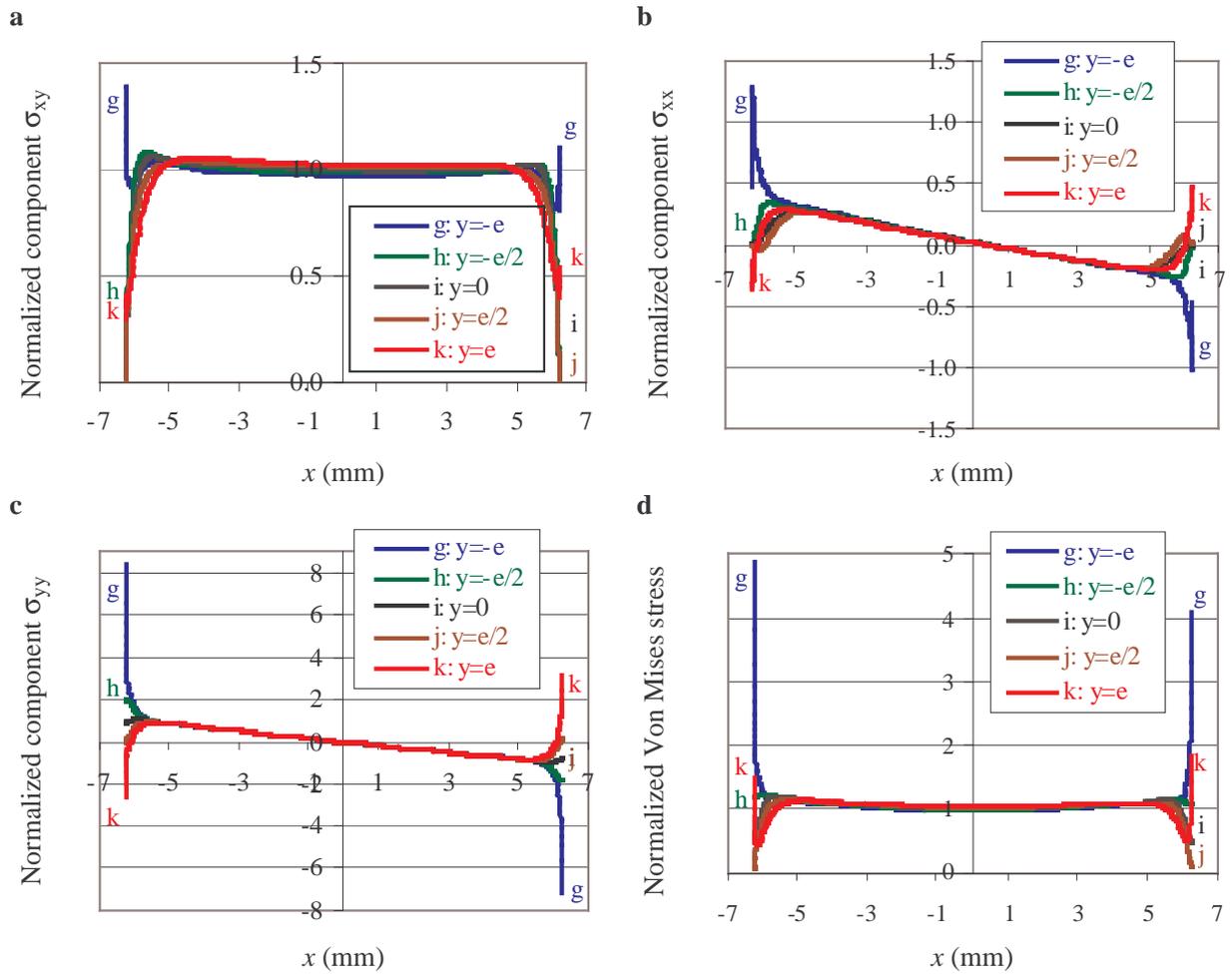
Figure 6. Stress distribution in the adhesive in double lap shear specimens; stress components (a) σ_{xy}, (b) σ_{xy}, (c) σ_{xy}, (d) von Mises equivalent stress, for different planes through the adhesive thickness

(a)

(b)
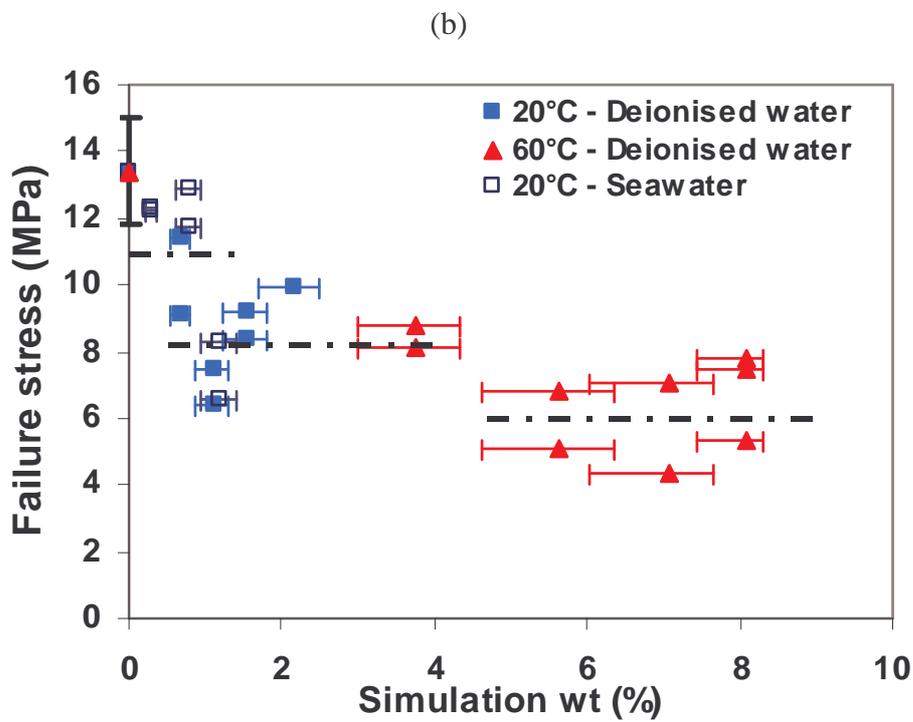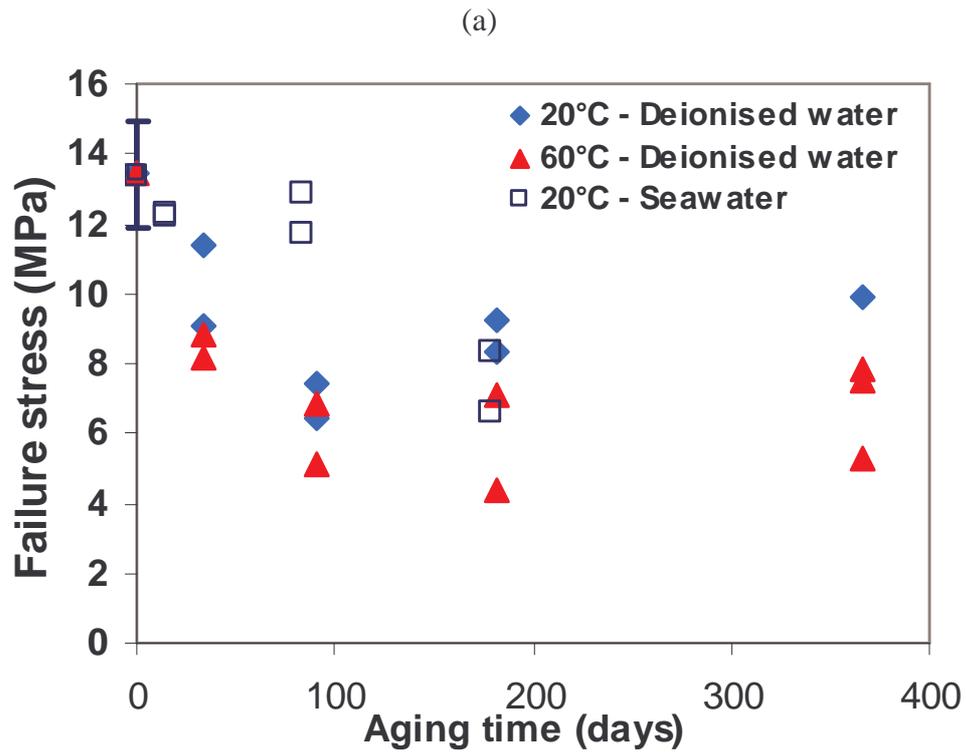
Figure 7. DLS failure stress evolution for aging in deionised water and seawater at 20 and 60°C plotted (a) versus aging time and (b) versus simulated weight gain.

(a)

(b)

(c)

(d)
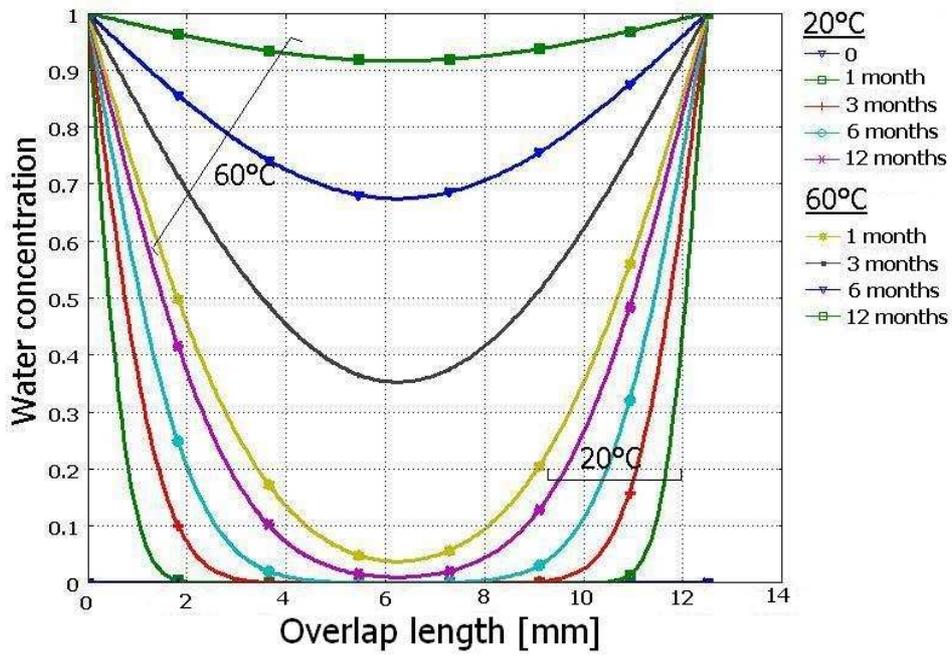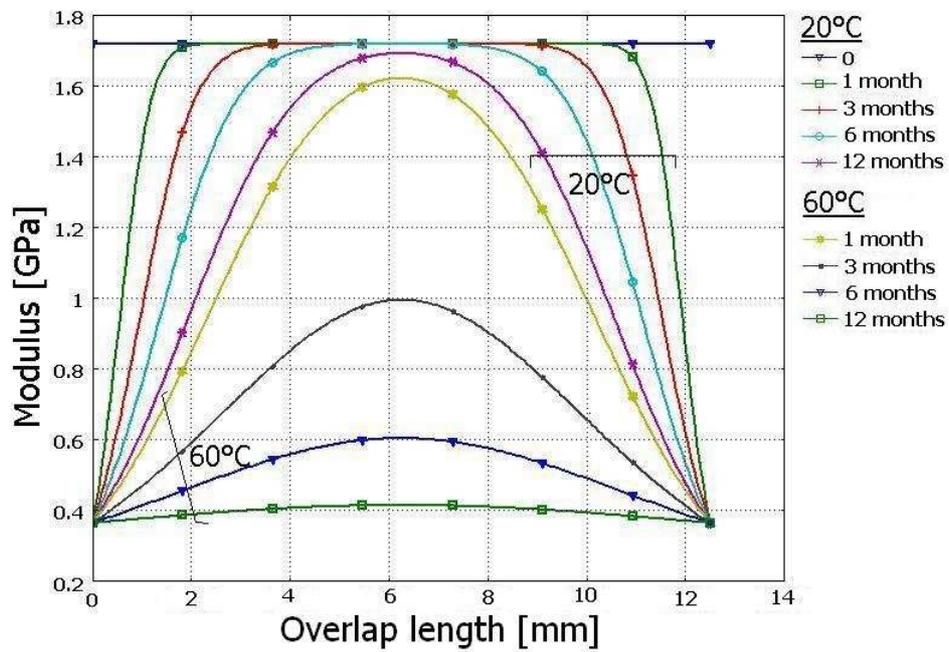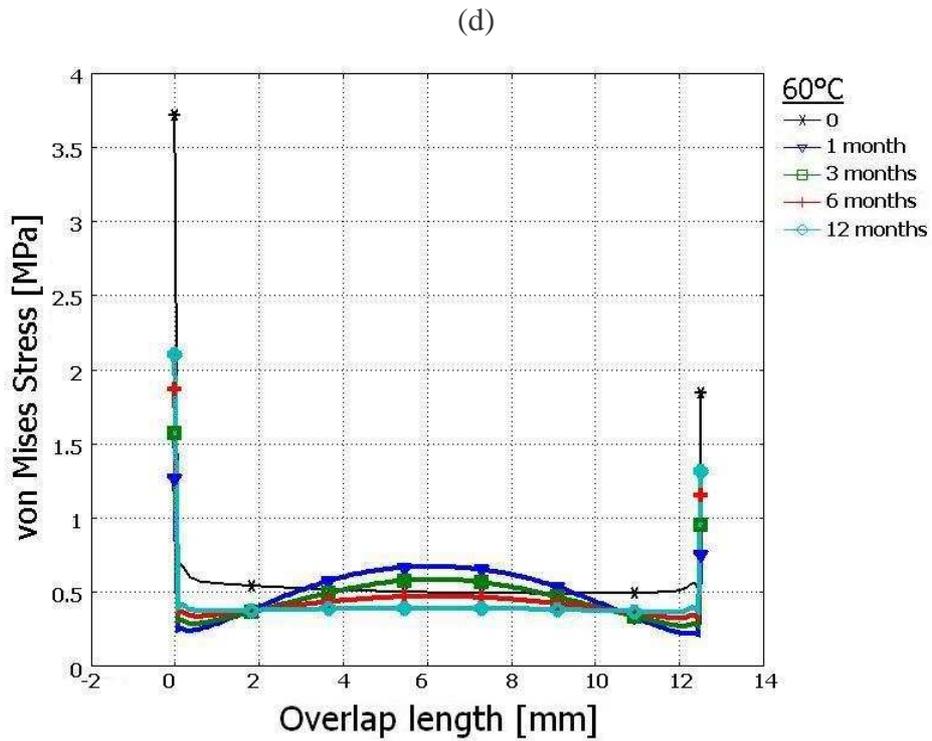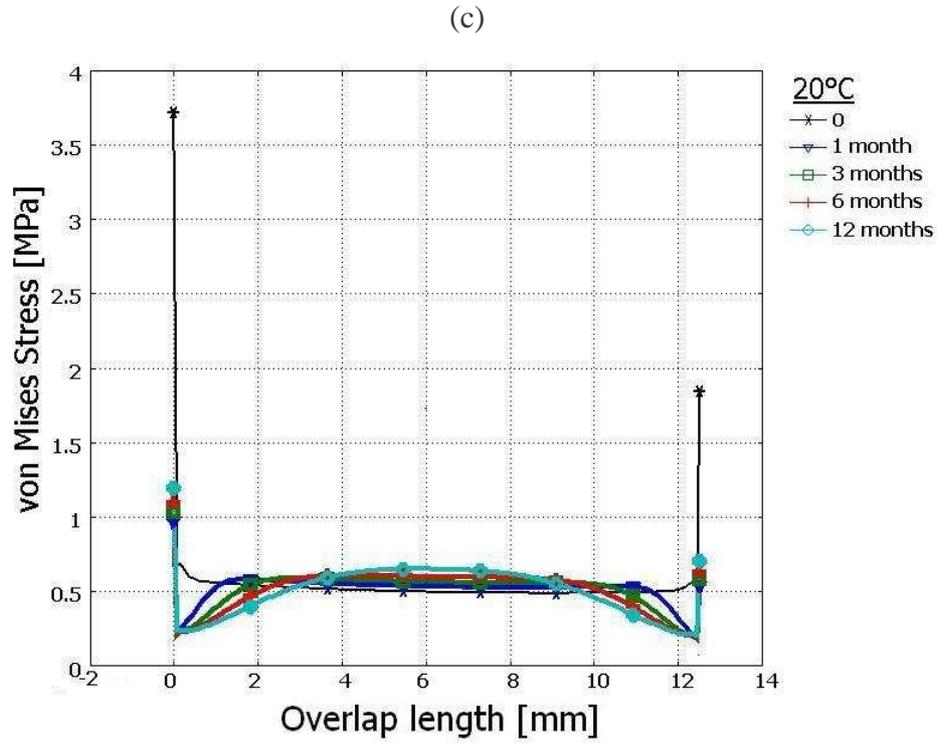
Figure 8. Evolution of (a) water concentration and (b) adhesive modulus versus DLS overlap length at different aging times in deionised water at 20 and 60°C and effect of aging on (c) von Mises stress along the interface AB (see Figure 5) at 20°C and (d) at 60°C .
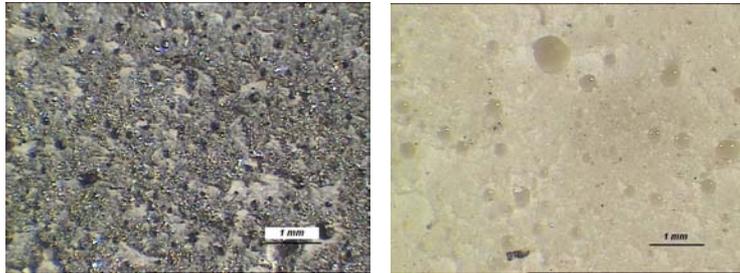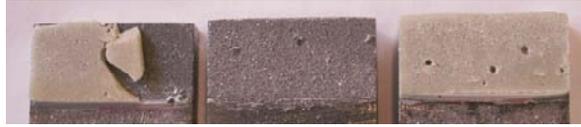
(a) Interfacial cohesive fracture, Unaged
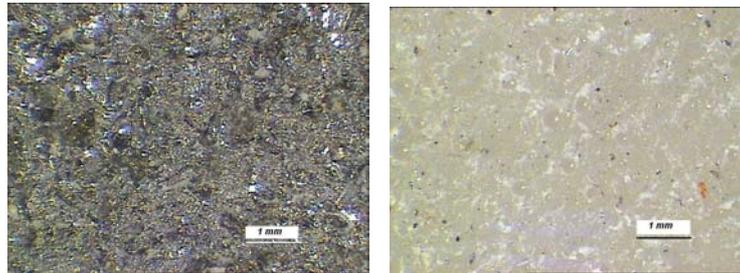
(b) Interfacial fracture, 3 months aging

Figure 9. Fracture surfaces of unaged (a) and aged (b) DLS specimens, overall view (upper) and details (lower)
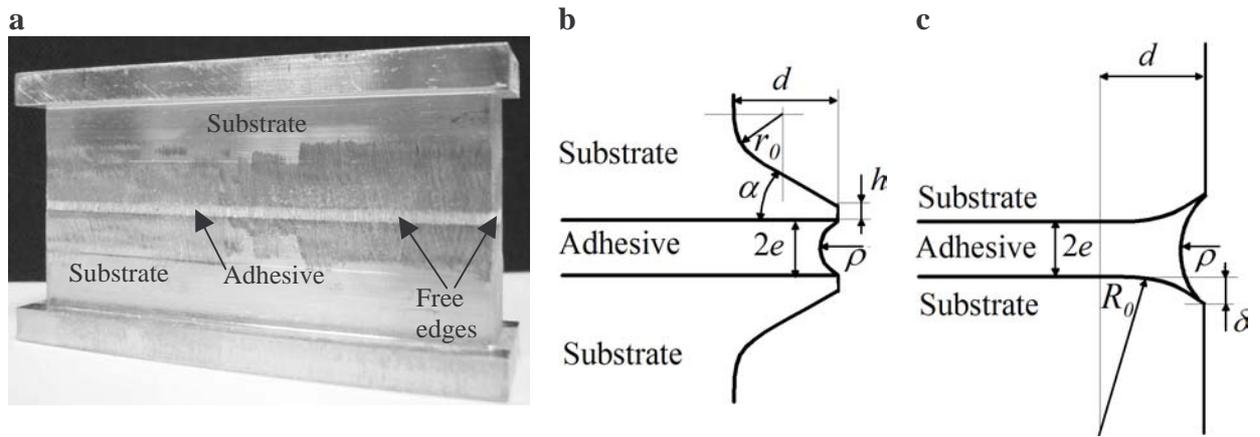
Figure 10. Geometries near the free edges of the joint. (a) bonded specimen, (b) substrates with original beaks, (c) substrates with new "inverse" geometry.
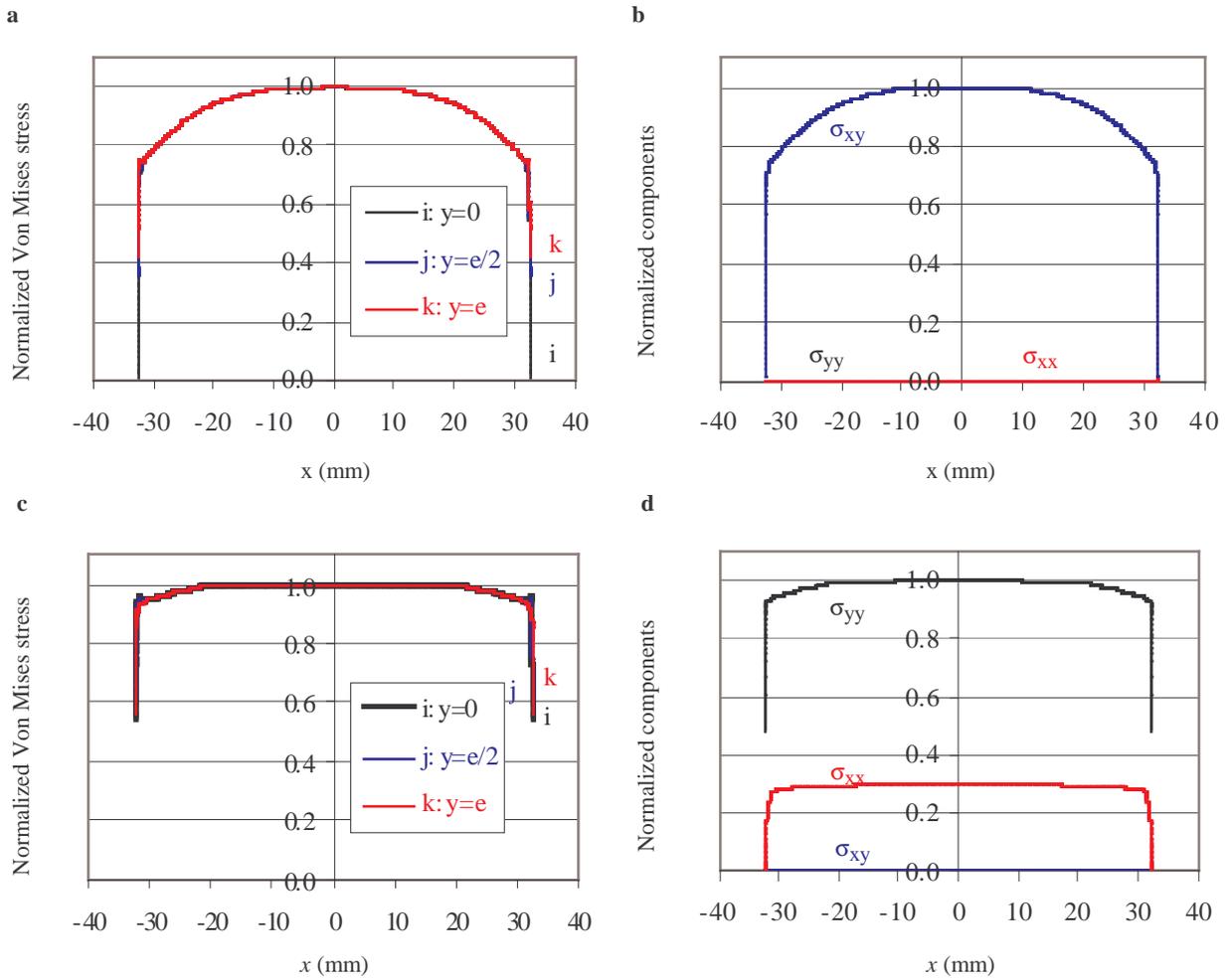
Figure 11. Stress analysis along the adhesive for modified Arcan fixture with inverse geometry, an adhesive thickness of 2 e = 0.5 mm, with straight edges $\rho = \infty$ and with the following parameters: $\delta = 0.2$ mm, d = 0.5 mm (Figure 10).

    (a) von Mises equivalent stress though the adhesive for shear loading,
    (b) stress components in the middle line of the adhesive for shear loading,
    (c) von Mises equivalent stress though the adhesive for tensile loading,
    (d) stress components in the middle line of the adhesive for tensile loading.
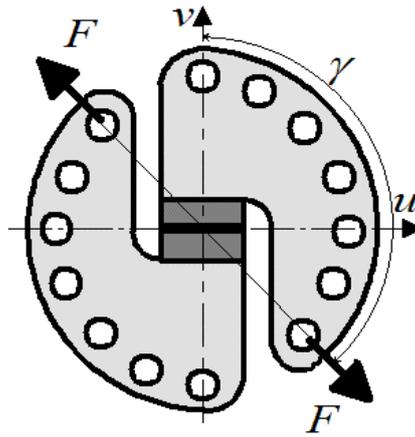
(a)
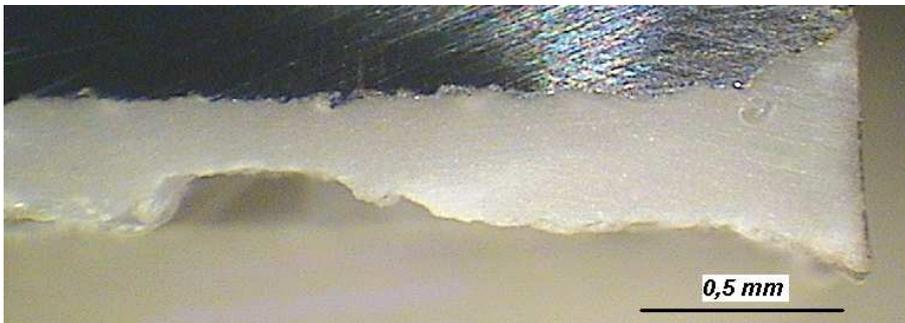
(b)

Figure 12. Arcan testing system, (a) test set-up and loading angles, (b) section through Arcan specimen after tensile test showing metallic substrate and chamfer above white adhesive layer.
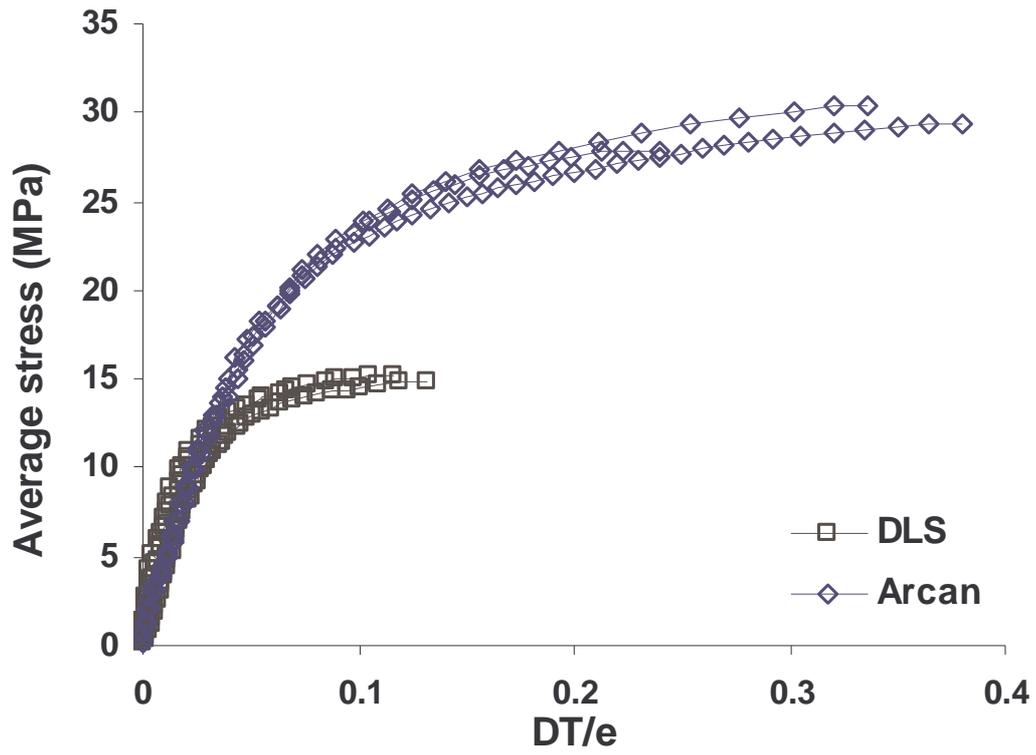
Figure 13. Comparison between the stress-deformation plots of the DLS and Arcan (shear) assemblies in the unaged (t_o) state.
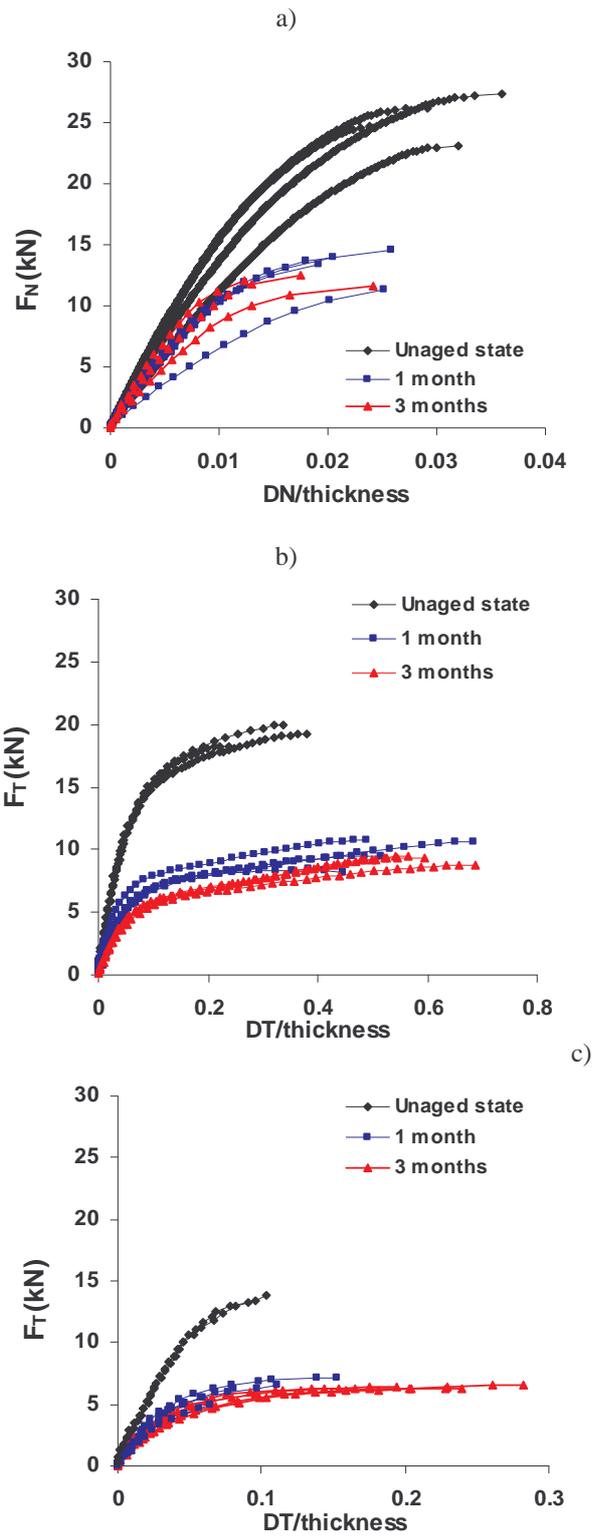
a)

Figure 14. Response of Arcan samples under (a) tension loading (b) shear loading (c) shear-tension loading, after different aging times in sea water.

(DN is displacement normal to specimen plane, DT is displacement tangential)
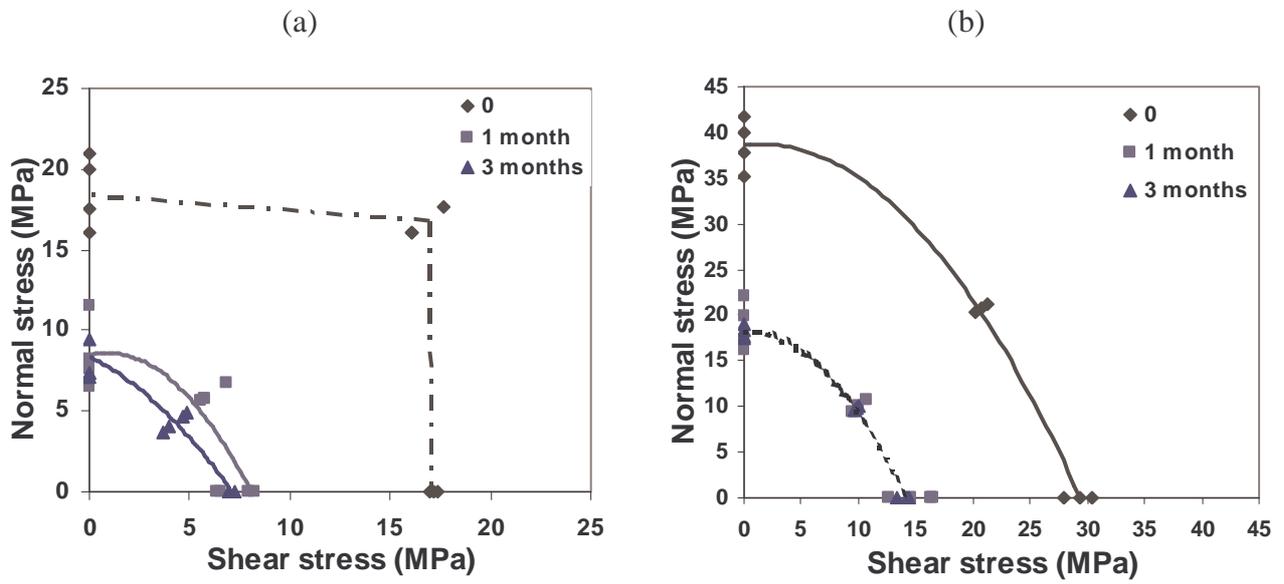
Figure 15. (a) Average yield and (b) failure stress envelopes before and after aging, Arcan specimens

Unaged state	**1 month**	**3 months**

Cohesive fracture

Mixed fracture

Mixed fracture

Tension loading

Interfacial cohesive fracture
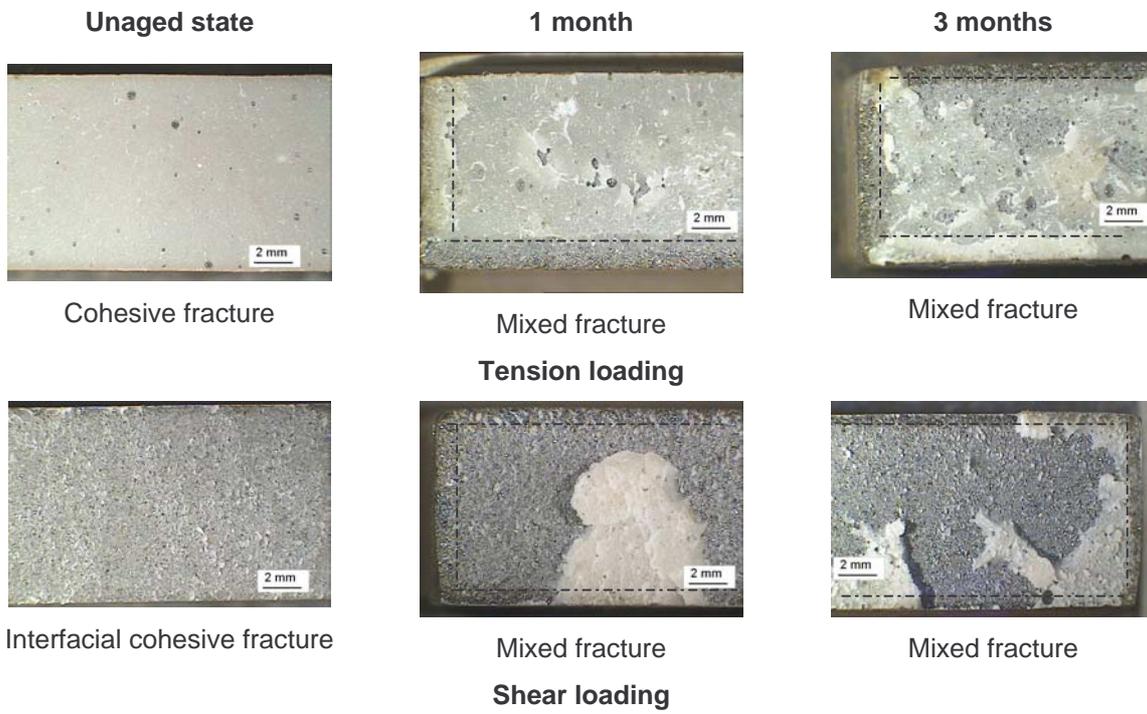
Mixed fracture

Mixed fracture

Shear loading

Figure 16. Fracture surfaces of the Arcan specimen before and after aging,
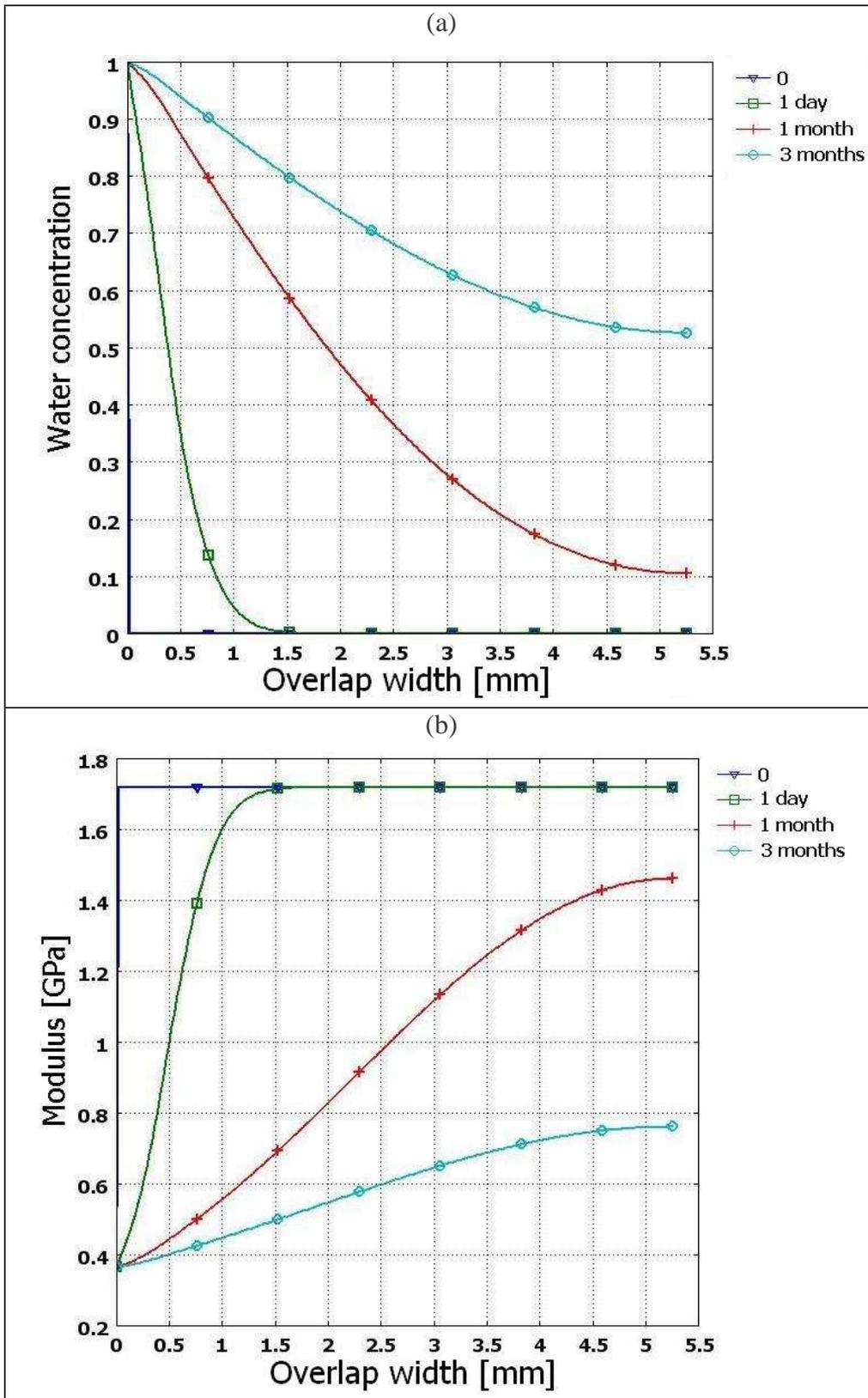
Figure 17. (a) Water concentration evolution, and (b) Adhesive modulus evolution along the Arcan adhesive joint half-width.
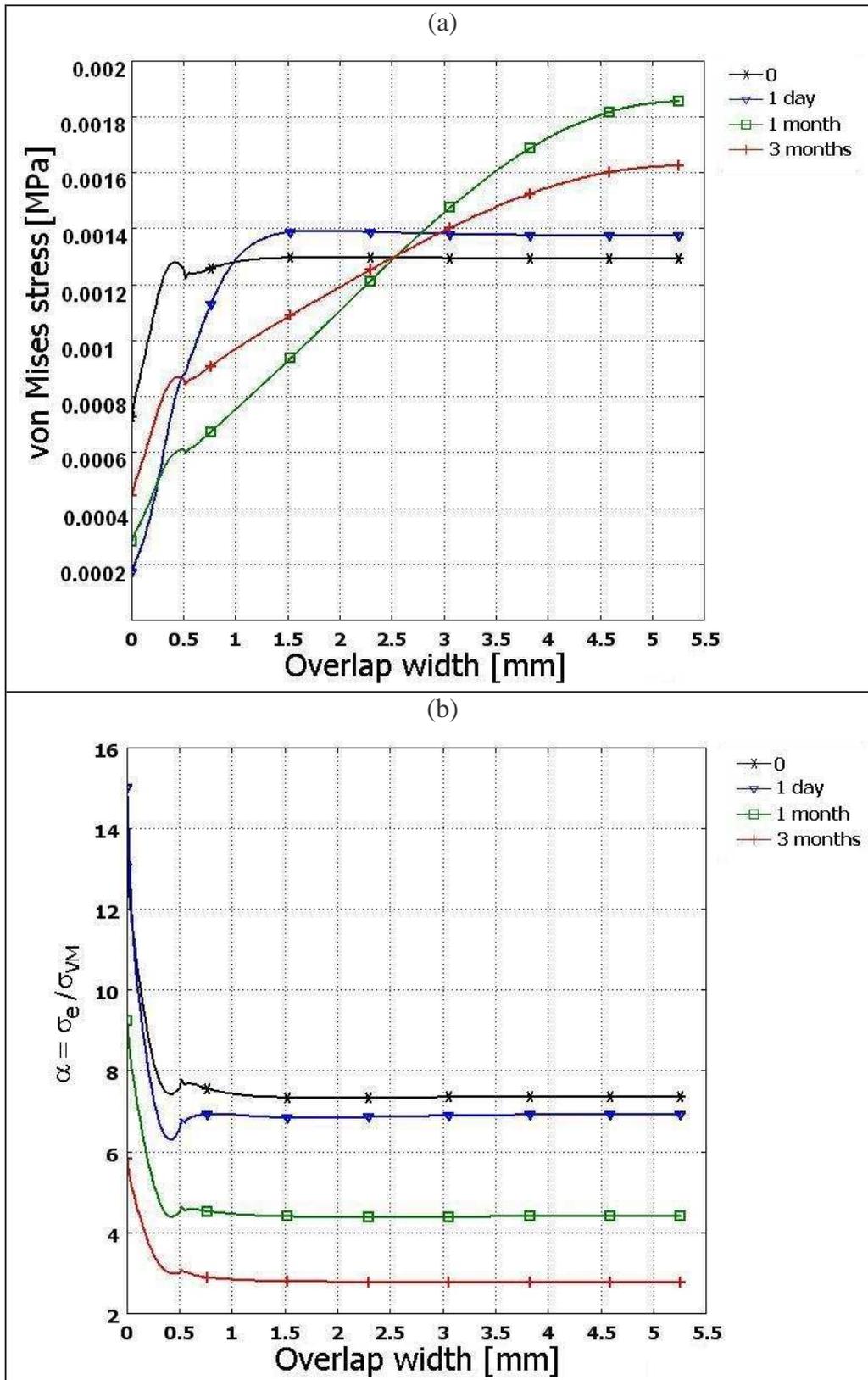
Figure 18 (a) Evolution of von Mises stress for unit load =1N and (b) evolution of the ratio α yield stress/von Mises stress along the Arcan joint half-width at different aging times.
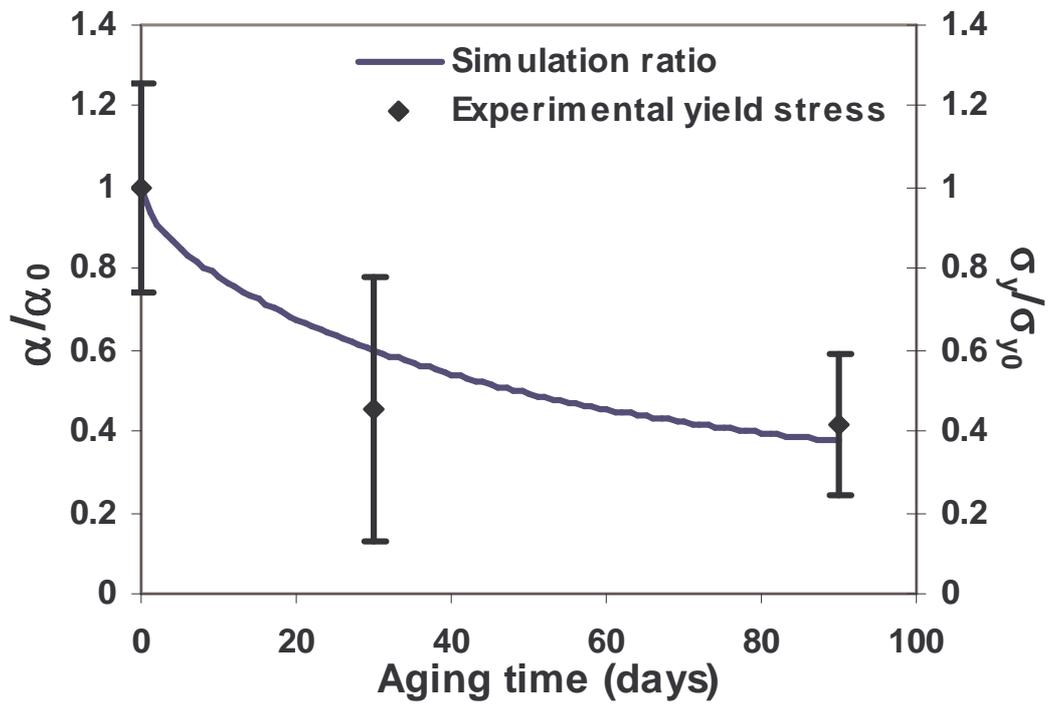
Figure 19. Comparison of model predictions for damage onset with experimental values of stress at end of linearity for Arcan tensile assembly, versus aging time, both normalized by initial unaged values (subscript o)